DALTON
FULL PAPER

Exploring the Lewis basicity of the metalloligand [$Pt_2(\mu\text{-}Se)_2(PPh_3)_4$] on metal substrates by electrospray mass spectrometry. Synthesis, characterization and structural studies of new platinum selenido phosphine complexes containing the {Pt_2Se_2} core

Jeremy S. L. Yeo,[a] **Jagadese J. Vittal,**[a] **William Henderson** *[b] **and T. S. Andy Hor** *[a]

[a] *Department of Chemistry, National University of Singapore, 3 Science Drive 3, Singapore 117543. E-mail: andyhor@nus.edu.sg*
[b] *Department of Chemistry, University of Waikato, Private Bag 3105, Hamilton, New Zealand. E-mail: w.henderson@waikato.ac.nz*

Received 6th June 2001, Accepted 26th October 2001
First published as an Advance Article on the web 20th December 2001

Electrospray Mass Spectrometry (ESMS) has been used as a tool to probe the reactivity of the metalloligand [$Pt_2(\mu\text{-}Se)_2(PPh_3)_4$] with metal substrates, which lead to the formation of charged coordination complexes *via* loss of halides or other labile ligands. Among the numerous metal substrates used in the displacement reactions are Au(anpy)Cl_2 (anpy = cyclometallated 2-anilinopyridyl), HgPhCl and $Pb(NO_3)_2$. Acid titration on the Lewis basic metalloligand leads to the identification and isolation of the doubly-protonated species, [$Pt_2(\mu\text{-}SeH)_2(PPh_3)_4$]$^{2+}$, whose sulfide analogue cannot be isolated. A three-step strategy is employed in the use of ESMS as a probe: (i) preliminary screening of the metalloligand with an array of acidic main group and transition group metal compounds, (ii) identification of potentially stable and isolable products formed *in situ* based on ion distribution and simulated isotope patterns and (iii) promising reactions are repeated on a laboratory scale, and target products are isolated and characterized. X-Ray diffraction studies have been performed on single crystals of [$Pt_2(\mu\text{-}SeH)_2(PPh_3)_4$][$ClO_4$]$_2$, [$Pt_2(\mu_3\text{-}Se)_2(PPh_3)_4(CdCl_2)$] and {$Pt_2(\mu_3\text{-}Se)_2(PPh_3)_4[Pb(NO_3)]$}{$NO_3$}. These results suggested that in general a parallel chemistry can be developed on the intermetallic selenides as on the sulfides. However, there are chemical and structural differences which are highlighted in this paper.

Introduction

Electrospray mass spectrometry (ESMS) is a soft ionization technique that has been employed extensively in the analysis of biomolecules such as proteins and oligonucleotides.[1] It has also been increasingly applied in the characterization of a range of inorganic and organometallic systems.[2,3] Recently, we discussed the development of ESMS as a rapid and convenient method to probe the chemistry of [$Pt_2(\mu\text{-}S)_2(PPh_3)_4$] **2** with a wide range of metal substrates.[4] This chemistry using $Pt_2(\mu\text{-}S)_2(PPh_3)_4$ as a metalloligand is now very well established,[5] but little was known until very recently on similar coordination chemistry of the {Pt_2Se_2} core.[6] In this paper, we repeat a parallel methodology applied to the selenide system. These are important materials as they are possible precursors for semiconducting materials.[7] Our effort could add a fresh pool of novel intermetallic selenide aggregates and clusters which are relatively rare in the current literature.[8] Using an approach aided by ESMS, we have been able to identify and synthesize an array of polynuclear selenide structures.

Results and discussion

(I) Reactivity of [$Pt_2(\mu\text{-}Se)_2(PPh_3)_4$]

Although the decomposition of **2** in chlorinated solvents is well known,[9] reports on [$Pt_2(\mu\text{-}Se)_2(PPh_3)_4$] **1** have only recently surfaced.[10] Besides their decomposition pathway and products, no other characteristics of these metalloligands have been investigated. Recently we reported the acid titration of **2** in an investigation of its Lewis basicity, yielding a novel monoprotonated complex [$Pt_2(\mu\text{-}S)(\mu\text{-}SH)(PPh_3)_4$][$PF_6$] upon metathesis with NH_4PF_6.[11] Initial reaction of **1** with a Lewis acid [$Ga(ClO_4)_3$] unexpectedly yielded a di-protonated product, [$Pt_2(\mu\text{-}SeH)_2(PPh_3)_4$][$ClO_4$]$_2$ **3**, which was structurally characterized (Fig. 1). The analogous product from **2** was a subject of speculation, but to date, it has not been isolated. The proton source was most probably generated by the Lewis acid in its commercially available aqueous solution form. Protonation of μ-E ligands (E = S, Se) is a general route to compounds containing μ-EH groups.[12] The structure of **3** shows a hinged {Pt_2Se_2} core with the two attached protons pointing away from one another. The dihedral angle of the four-membered Pt_2Se_2 ring is acute (71.9°), in large contrast to those in [$Pt_2(\mu\text{-}Se)_2(PPh_3)_4$] (180°),[13] tin(IV)-[$Pt_2(\mu\text{-}Se)_2(PPh_3)_4$] complexes[6] (128–130°) and also [$Pt_2(\mu\text{-}S)(\mu\text{-}SH)(PPh_3)_4$][$PF_6$][11] (135°). Acid titration using HCl was subsequently performed on **1** and the NMR analysis of the product matched that obtained from Ga^{3+}. The identity of the di-protonated complex is reconfirmed by subsequent reaction of **1** with HPF_6. Careful addition of acid to **1** (1 : 1 ratio) yielded a mixture of both mono- and di-protonated products.

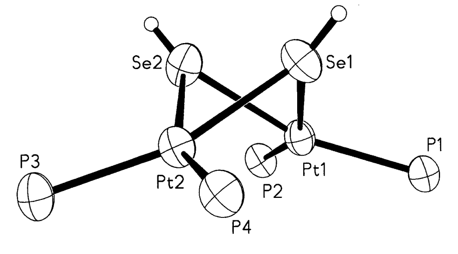

Fig. 1 Molecular structure of the cation of [$Pt_2(\mu\text{-}SeH)_2(PPh_3)_4$][$ClO_4$]$_2$ **3**. The phenyl rings are omitted for clarity.

DOI: 10.1039/b104996h

(II) Three-step synthesis strategy employing ESMS as probe

The reactions of the metalloligand $Pt_2(\mu\text{-}Se)_2(PPh_3)_4$ **1** with a wide range of metal complexes have been initially screened using electrospray mass spectrometry (ESMS). The trends observed from our recent report involving **1** and Sn(IV) substrates[6] are also seen in this series of ESMS-monitored reactions. The general observations include: (i) Displacement of one or two labile ligands on the metal substrates through nucleophilic attack of the Se atoms of **1** which then leads to the formation of cationic aggregates. (ii) Most reactions gave both mono- and di-cations through loss of one and two ligands respectively. Di-cations became the dominant species when more substrate was added to these reaction mixtures. As the cone voltage was increased, mono-cations were commonly the dominant peaks in the spectra. (iii) The common fragmentation route (when high cone voltages of 60 or 80 V are applied) involves loss of PPh_3 ligands. (iv) Detection of peaks at *m*/*z* 799 and 1598, assigned as $[\mathbf{1} + 2H]^{2+}$ and $[\mathbf{1} + H]^{+}$ respectively, were normally observed when reactions did not occur, or **1** was in excess. In this report, only those reactions that give unexpected and interesting products and fragmentation pathways are singled out and discussed in detail. Schlenk-flask syntheses and characterization of these charged aggregates and those deduced from the ESMS spectra were followed up. The isolated products were characterized by the conventional NMR and single-crystal X-ray diffraction analyses. The results demonstrate that ESMS is valuable not only in monitoring the progress of reactions, it also provides a preliminary "screening" of the feasibility of reactions prior to preparative scale syntheses. All reactions performed under ESMS and laboratory-scale conditions are summarized in the tables and Experimental section. The usual observations of the loss of PPh_3 ligands at high cone voltages (60–80 V) are excluded from the ESMS discussions.

(a) Reactions between 1 and gold substrates. The ESMS data for this series of reactions are summarized in Table 1. The ease of displacement of chloride ligands on the gold substrates by **1** depends on the electron-donating as well as chelating ability of the ligands on the substrates.

Reaction between **1** and $AuCl(PPh_3)$ gave a clean spectrum with a peak at *m*/*z* 2056 at moderately low cone voltages (20–40 V), attributed to $\{\mathbf{1}[Au(PPh_3)]\}^{+}$. When the cone voltage was further increased to 60 V, fragmentation occurred through loss of one PPh_3 ligand, resulting in either the detection of mono-cation $\{(\mathbf{1} - PPh_3)[Au(PPh_3)]\}^{+}$ or $[\mathbf{1}(Au)]^{+}$.

Reaction of **1** with $Au(anpy)Cl_2$ **I** (anpy = cyclometallated 2-anilinopyridyl) resulted in detection of $\{\mathbf{1}[Au(anpy)]\}^{2+}$ and $\{(\mathbf{1} - PPh_3)_2[Au(anpyH)]\}^{3+}$ **4** at cone voltages between 20 and 60 V. The proposed structure of **4** is shown in Fig. 2, together with the observed and calculated isotope patterns. The identity of the tri-cation is clearly demonstrated by the corresponding match between the two isotope patterns. Protonation by the solvent presumably takes place on the nitrogen atom of the formerly cyclometallated anilinopyridine ligand to give **4**. Such protonation of the cyclometallated ligands on Au(III) ions has been observed previously.[14]

For the reaction between **1** and $Au(tolpy)Cl_2$ **II** (tolpy = cyclometallated *p*-tolylpyridyl), $\{\mathbf{1}[Au(tolpy)]\}^{2+}$ was detected at 20 V. Further increasing the cone voltage to 40 V gave a significant peak at *m*/*z* 1288 (41% relative intensity *cf.* the most intense peak $\{\mathbf{1}[Au(tolpy)]\}^{2+}$), possibly attributed to $\{(\mathbf{1} - PPh_3)[Au(tolpyH)][PtSe_2(PPh_3)_2] + H\}^{2+}$ **5**. Solvent protonation thus appears to occur again on the nitrogen atom of the tolylpyridine-derived ligand.

Reaction between **1** and $Au(tolpyH)Cl_3$ **III** or $[AuCl_4][NMe_4]$ is less spontaneous compared to the three earlier mentioned gold substrates. At a low cone voltage (20 V), $[Pt(PPh_3)_2Cl]^{+}$, $[(\mathbf{1})_2Au]^{3+}$, $[(\mathbf{1} - PPh_3)_2(AuCl_2) + H]^{2+}$ and $[\mathbf{1}(AuCl_2)]^{+}$ were detected. At this voltage, $[Pt(PPh_3)_2Cl]^{+}$ and $[\mathbf{1}(AuCl_2)]^{+}$ were equally dominant. $[(\mathbf{1})_2Au]^{3+}$ **6**, being surprisingly detected at reasonable intensity, might be attributed to the preferred stabilization of the 'naked' Au^{3+} ion through coordination with two units of $Pt_2(\mu\text{-}Se)_2(PPh_3)_4$. Such stabilization has been observed in cyclometallated gold(III) complexes which form stable derivatives with thiolate[15] and thiolate-type[14] ligands. At a high cone voltage (60 V), $[Pt(PPh_3)_2Cl]^{+}$ became the dominant ion, together with the platinum cation containing a cyclometallated triphenylphosphine ligand, $\{Pt(PPh_3)[PPh_2(C_6H_4)]\}^{+}$. This cation was discussed in detail in a recent paper.[3]

(b) Reactions between 1 and Group 12 metal (mercury, cadmium) substrates. Group 12 metals, especially mercury,[16] have a very strong affinity for both sulfur and selenium. ESMS data for reactions between **1** and Group 12 metal substrates are summarized in Table 2.

Reaction between **1** and thiomersal **IV** ($EtHgSC_6H_4CO_2Na$) was not straightforward. Thiomersal is a convenient source of the $[HgEt]^{+}$ cation. At low cone voltages (20–40 V), the expected ions $[\mathbf{1}(HgEt)]^{+}$ **7** and $[\mathbf{1}(HgEt)_2]^{2+}$ **8** were detected along with $[Pt(PPh_3)_2(\eta^2\text{-}SC_6H_4CO_2) + H]^{+}$ and $[Pt(PPh_3)_2(\eta^2\text{-}SC_6H_4CO_2) + Na]^{+}$. The detection of the mononuclear platinum thiosalicylate ions can be explained by Scheme 1, with $Se(HgEt)_2$ being a proposed byproduct. The synthesis and characterization of $[Pt(PPh_3)_2(\eta^2\text{-}SC_6H_4CO_2)]$ was reported in a recent paper,[3] including the thiolate exchange reaction between *cis*-$[PtCl_2(PPh_3)_2]$ and thiomersal, giving $[Pt(PPh_3)_2(\eta^2\text{-}SC_6H_4CO_2)]$ (and presumably HgEtCl).[17]

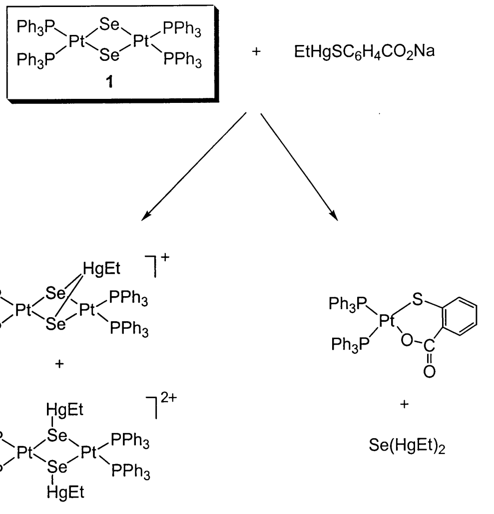

Scheme 1 Mechanism depicting reaction between **1** and thiomersal.

Complex **1** reacts with ferrocenyl mercury chloride **V** to give $[\mathbf{1}(HgFc)]^{+}$, $[\mathbf{1}(HgFc)_2]^{2+}$ and $[(\mathbf{1})_2Hg]^{2+}$ **9** at a cone voltage of 20 V. Although $[(\mathbf{1})_2Hg]^{2+}$ was detected as a minor product under ESMS conditions, we have managed to isolate this cationic product as its PF_6^{-} salt under laboratory-scale conditions, solely from the decomposition of $[\mathbf{1}(HgFc)][PF_6]$ in CH_2Cl_2 after a week. The formation of $[(\mathbf{1})_2Hg][PF_6]_2$ points to the stabilization of a 'naked' Hg^{2+} ion by two molecules of **1**. The source of this Hg^{2+} cation originated from the cleavage of the Hg–Fc bond in pre-purified **V**, not as an impurity. A similar observation was absent in our parallel study with **2**.[4] $\{[Pt_2(\mu_3\text{-}S)_2(PPh_3)_4]_2(Hg)\}^{2+}$ has been reported by Mingos *et al.*,[18] however, there is no report on the selenium analogue. Complex **1** also reacted with $HgCl_2(PPh_3)_2$ or $HgBr_2(dppe)$ to give **9**, observed at cone voltages in the range of 20–60 V. $Hg(ClO_4)_2$ was also used as a substrate for **1**, with the intention to isolate **9** cleanly. At a cone voltage of 20 V, the reaction gave the only distinct peak at *m*/*z* 1698 pertaining to **9**.

Table 1 ESMS data for reactions between $[Pt_2(\mu\text{-}Se)_2(PPh_3)_4]$ **1** and gold substrates

Combinations	Cone voltage/V	Major ions (*m*/*z*, %)
$\mathbf{1} + AuCl(PPh_3)$	20–40	$\{\mathbf{1}[Au(PPh_3)]\}^+$ (2056, 100)
	60	$\{(\mathbf{1} - PPh_3)[Au(PPh_3)]\}^+$ or $[(\mathbf{1}(Au)]^+$ (1794, 56), $\{\mathbf{1}[Au(PPh_3)]\}^+$ (2056, 100)
	80	$\{(\mathbf{1} - 2PPh_3)[Au(PPh_3)]\}^+$ or $[(\mathbf{1} - PPh_3)(Au)]^+$ (1532, 16), $\{(\mathbf{1} - PPh_3)[Au(PPh_3)]\}^+$ or $[(\mathbf{1}(Au)]^+$ (1794, 100), $\{\mathbf{1}[Au(PPh_3)]\}^+$ (2056, 30)
$\mathbf{1} + Au(anpy)Cl_2$	20–60	$\{\mathbf{1}[Au(anpy)]\}^{2+}$ (982, 100), $\{(\mathbf{1} - PPh_3)_2[Au(anpyH)] + H\}^{3+}$ (1013, 5)
$\mathbf{1} + Au(tolpy)Cl_2$	20	$\{\mathbf{1}[Au(tolpy)]\}^{2+}$ (982, 100)
	40	$\{\mathbf{1}[Au(tolpy)]\}^{2+}$ (982, 100), $\{(\mathbf{1} - PPh_3)[Au(tolpyH)][PtSe_2(PPh_3)_2] + H\}^{2+}$ (1288, 41)
	60	$\{\mathbf{1}[Au(tolpy)]\}^{2+}$ (982, 100), $\{(\mathbf{1} - PPh_3)[Au(tolpyH)][PtSe_2(PPh_3)_2] + H\}^{2+}$ (1288, 22), $\{(\mathbf{1} - 2PPh_3)\text{-}[Au(tolpyH)][PtSe_2(PPh_3)_2] + H\}^{2+}$ (1157, 33)
	80	$\{\mathbf{1}[Au(tolpy)]\}^{2+}$ (982, 11), $\{(\mathbf{1} - PPh_3)[Au(tolpyH)][PtSe_2(PPh_3)_2] + H\}^{2+}$ (1288, 7), $\{(\mathbf{1} - 2PPh_3)\text{-}[Au(tolpyH)][PtSe_2(PPh_3)_2] + H\}^{2+}$ (1157, 100)
$\mathbf{1} + Au(tolpyH)Cl_3$	20	$[Pt(PPh_3)_2Cl]^+$ (754, 99), $[\mathbf{1} + 2H]^{2+}$ (799, 63), $[(\mathbf{1})_2Au]^{3+}$ (1130, 83), $[(\mathbf{1} - PPh_3)_2(AuCl_2) + H]^{2+}$ (1469, 79), $[\mathbf{1}(AuCl_2)]^+$ (1865, 100)
	60	$[Pt(PPh_3)_2Cl]^+$ (754, 99), $[\mathbf{1} + 2H]^{2+}$ (799, 93), $[(\mathbf{1})_2Au]^{3+}$ (1130, 3), $[(\mathbf{1} - PPh_3)_2(AuCl_2) + H]^{2+}$ (1469, 17), $[\mathbf{1}(AuCl_2)]^+$ (1865, 100)
	80	$[Pt(PPh_3)(PPh_2C_6H_4)]^+$ (718, 100), $[Pt(PPh_3)_2Cl]^+$ (754, 48), $[\mathbf{1} + 2H]^{2+}$ (799, 42), $[(\mathbf{1} - PPh_3)_2(AuCl_2) + H]^{2+}$ (1469, 5), $[\mathbf{1}(AuCl_2)]^+$ (1865, 95)
$\mathbf{1} + [NMe_4][AuCl_4]$	20	$[Pt(PPh_3)_2Cl]^+$ (754, 100), $[(\mathbf{1})_2Au]^{3+}$ (1130, 16), $[(\mathbf{1} - PPh_3)_2(AuCl_2) + H]^{2+}$ (1469, 25), $[\mathbf{1}(AuCl_2)]^+$ (1865, 85)
	60	$[Pt(PPh_3)(PPh_2C_6H_4)]^+$ (718, 25), $[Pt(PPh_3)_2Cl]^+$ (754, 100), $[(\mathbf{1} - PPh_3)_2(AuCl_2) + H]^{2+}$ (1469, 15), $[\mathbf{1}(AuCl_2)]^+$ (1865, 75)
	80	$[Pt(PPh_3)(PPh_2C_6H_4)]^+$ (718, 100), $[Pt(PPh_3)_2Cl]^+$ (754, 69), $[(\mathbf{1} - PPh_3)_2(AuCl_2) + H]^{2+}$ (1469, 3), $[\mathbf{1}(AuCl_2)]^+$ (1865, 67)

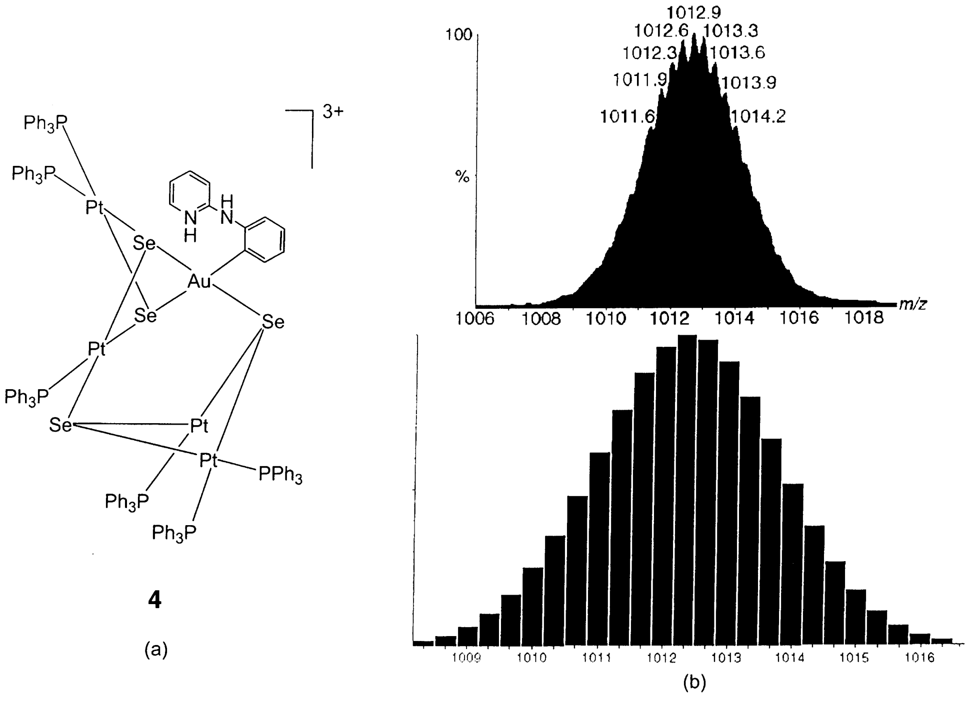

4

(a)

(b)

Fig. 2 (a) Proposed structure of **4**. (b) Isotope pattern of **4** (above), simulated pattern from isotope program (below).

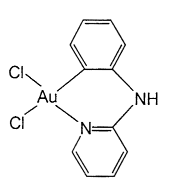

Cyclometallated 2-anilinopyridyl gold dichloride[24]
$[Au(anpy)Cl_2]$ I

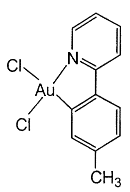

Cyclometallated *p*-tolylpyridyl gold dichloride[25]
$[Au(tolpy)Cl_2]$ II

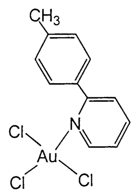

p-tolylpyridine gold trichloride[25]
$[Au(tolpyH)Cl_3]$ III

Complex **1** reacts with $HgCl(BzNMe_2)$ **VI** at 20 V to give $\{\mathbf{1}[Hg(BzNMe_2)]_2\}^{2+}$ and $\{\mathbf{1}[Hg(BzNMe_2)]\}^+$, the latter further being protonated (by the solvent) to give $\{\mathbf{1}[Hg(BzNHMe_2)]\}^{2+}$ at *m*/*z* 966. Increasing the cone voltage to 40 V eliminated $\{\mathbf{1}[Hg(BzNMe_2)]_2\}^{2+}$, and further eliminated $\{\mathbf{1}[Hg(BzNHMe_2)]\}^{2+}$ at 80 V to give $\{\mathbf{1}[Hg(BzNMe_2)]\}^+$ as the dominant ion. Similar

Table 2 ESMS data for reactions between $[Pt_2(\mu\text{-}Se)_2(PPh_3)_4]$ **1** and Group 12 substrates

Combinations	Cone voltage/V	Major ions (*m*/*z*, %)
1 + HgPhCl	20	$[\mathbf{1}(HgPh)_2]^{2+}$ (1076, 33), $[\mathbf{1}(HgPh)]^+$ (1875, 100)
	60	$[\mathbf{1}(HgPh)]^+$ (1875, 100)
	80	$[(\mathbf{1} - 2PPh_3)(HgPh)]^+$ (1351, 9), $[(\mathbf{1} - PPh_3)(HgPh)]^+$ (1613, 15), $[\mathbf{1}(HgPh)]^+$ (1875, 100)
1 + Thiomersal	20	$[Pt(PPh_3)_2(\eta^2\text{-}SC_6H_4CO_2) + H]^+$ (873, 10), $[Pt(PPh_3)_2(\eta^2\text{-}SC_6H_4CO_2) + Na]^+$ (896, 47), $[\mathbf{1}(HgEt)_2]^{2+}$ (1028, 19), $[\mathbf{1}(HgEt)]^+$ (1827, 100)
	40	$[Pt(PPh_3)_2(\eta^2\text{-}SC_6H_4CO_2) + H]^+$ (873, 13), $[Pt(PPh_3)_2(\eta^2\text{-}SC_6H_4CO_2) + Na]^+$ (896, 47), $[\mathbf{1}(HgEt)_2]^{2+}$ (1028, 8), $[\mathbf{1}(HgEt)]^+$ (1827, 100)
	60	$[Pt(PPh_3)_2(\eta^2\text{-}SC_6H_4CO_2) + H]^+$ (873, 13), $[Pt(PPh_3)_2(\eta^2\text{-}SC_6H_4CO_2) + Na]^+$ (896, 42), $[\mathbf{1}(HgEt)]^+$ (1827, 100)
	80	$[Pt(PPh_3)_2(\eta^2\text{-}SC_6H_4CO_2) + H]^+$ (873, 5), $[Pt(PPh_3)_2(\eta^2\text{-}SC_6H_4CO_2) + Na]^+$ (896, 28), $[(\mathbf{1} - 2PPh_3)(HgEt)]^+$ (1303, 19), $[(\mathbf{1} - PPh_3)(HgEt)]^+$ (1565, 23), $[\mathbf{1}(HgEt)]^+$ (1827, 100)
1 + HgFcCl	20	$[\mathbf{1}(HgFc)_2]^{2+}$ (1184, 17), $[(\mathbf{1})_2Hg]^{2+}$ (1698, 7), $[\mathbf{1}(HgFc)]^+$ (1983, 100)
	80	$[\mathbf{1}(HgFc)]^+$ (1875, 100)
1 + $HgCl(BzNMe_2)$	20	$[\mathbf{1}(HgBzNHMe_2)]^{2+}$ (966, 100), $[\mathbf{1}(HgBzNMe_2)_2]^{2+}$ (1132, 11), $[\mathbf{1}(HgBzNMe_2)]^+$ (1931, 87)
	40	$[\mathbf{1}(HgBzNHMe_2)]^{2+}$ (966, 71), $[\mathbf{1}(HgBzNMe_2)]^+$ (1931, 100)
	80	$[\mathbf{1}(HgBzNMe_2)]^+$ (1931, 100)
1 + HgCl(*p*-OMe-$BzNMe_2$)	20	$\{\mathbf{1}[Hg(p\text{-}OMe\text{-}BzNHMe_2)]\}^{2+}$ (982, 100), $\{\mathbf{1}[Hg(p\text{-}OMe\text{-}BzNMe_2)]\}^+$ (1962, 13)
	40	$\{\mathbf{1}[Hg(p\text{-}OMe\text{-}BzNHMe_2)]\}^{2+}$ (982, 100), $\{\mathbf{1}[Hg(p\text{-}OMe\text{-}BzNMe_2)]\}^+$ (1962, 25)
	60	$\{\mathbf{1}[Hg(p\text{-}OMe\text{-}BzNHMe_2)]\}^{2+}$ (982, 100), $\{\mathbf{1}[Hg(p\text{-}OMe\text{-}BzNMe_2)]\}^+$ (1962, 67)
	80	$\{\mathbf{1}[Hg(p\text{-}OMe\text{-}BzNMe_2)]\}^+$ (1962, 100)
1 + Fluorescein$[Hg(OAc)]_2$	20–60	$\{\mathbf{1}[Fluorescein(Hg)_2]\}^{2+}$ (1164, 100)
1 + $HgCl_2(PPh_3)_2$	20	$[\mathbf{1} + 2H]^{2+}$ (799, 10), $[\mathbf{1} + H]^+$ (1598, 15), $[(\mathbf{1})_2Hg]^{2+}$ (1698, 100)
	40–60	$[(\mathbf{1})_2Hg]^{2+}$ (1698, 100)
1 + $HgBr_2$(dppe)	20–60	$[(\mathbf{1})_2Hg]^{2+}$ (1698, 100)
1 + $Hg(ClO_4)_2$	20–60	$[(\mathbf{1})_2Hg]^{2+}$ (1698, 100)
1 + $CdCl_2$	20	$[\mathbf{1}(CdCl)]^+$ (1745, 100)
	80	$[(\mathbf{1} - PPh_3)(CdCl)]^+$ (1483, 5), $[\mathbf{1}(CdCl)]^+$ (1745, 100)

protonation on the amino group was also observed for the reaction between **1** and HgCl(*p*-OMeBzNMe$_2$) **VII**. However, the protonated ion was dominant over $\{\mathbf{1}[Hg(p\text{-}OMeBzNMe_2)]\}^+$ at low cone voltages. At 60 V, competition came between these two ions and at 80 V, $\{\mathbf{1}[Hg(p\text{-}OMeBzNMe_2)]\}^+$ emerged as the dominant ion.

For the reaction between **1** and $CdCl_2$, a single dominant ion $[\mathbf{1}(CdCl)]^+$ was observed between 20–60 V. A further increase of the cone voltage to 80 V only gave an insignificant peak at *m*/*z* 1483 (5% relative intensity *cf.* the most intense peak $[\mathbf{1}(CdCl)]^+$) attributed to $[(\mathbf{1} - PPh_3)(CdCl)]^+$. The synthesis and characterization of the product of this reaction (discussed in the Experimental section) was followed up on a preparative scale and instead of obtaining a cationic product containing $[\mathbf{1}(CdCl)]^+$, a neutral compound was prepared and structurally characterized as $[Pt_2(\mu_3\text{-}Se)_2(PPh_3)_4(CdCl_2)]$ **11e** (with a disordered CH_2Cl_2 and two H_2O solvates). The neutral compound was re-analyzed under ESMS conditions (dissolved in CH_2Cl_2, using MeOH as mobile phase) and the results matched those discussed above. Fig. 3 shows the structure of **11e** and its pertinent bond distances and angles are given in Table 3. X-Ray analysis revealed that compound **11e** consists of a $\{CdCl_2\}$ moiety coordinated to the metalloligand $[Pt_2(\mu\text{-}Se)_2(PPh_3)_4]$, forming a distorted square-based pyramidal aggregate (cadmium atom on the $\{Pt_2Se_2\}$ core) with a two-fold symmetry along the center axis (referenced to the cadmium atom). The dissociation of one chloride from compound **11e** with the detection of $[\mathbf{1}(CdCl)]^+$ as the dominant ion under ESMS conditions is further supported by our recent work on $\{Pt_2(\mu_3\text{-}S)_2(PPh_3)_4[CdCl(bipy)]\}\{PF_6\}$[19] where only one chloride on the coordinated cadmium was substituted by a bipyridyl ligand. Similar halide dissociation from a range of neutral metal complexes to give $[M - Cl]^+$ under ESMS conditions has also been reported recently.[20] Thus, ESMS is unable to distinguish between neutral dihalide complexes and cationic monohalide complexes derived from them by loss of a halide; the two

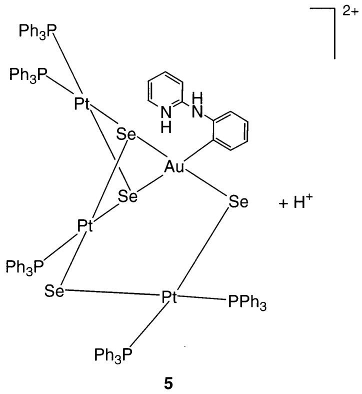

5

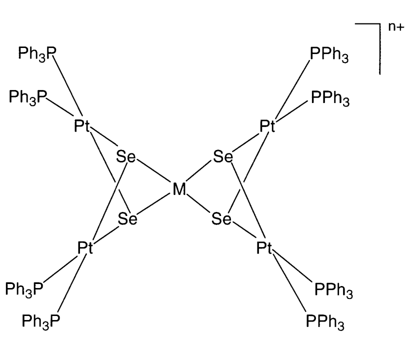

6; M = Au, n = 3

9; M = Hg, n = 2

Table 3 Selected bond lengths (Å) and angles (°) for compound **11e**

Pt(1)–P(1)	2.2727(17)	Pt(1A)–Se(1)	2.4917(7)
Pt(1)–P(2)	2.2885(18)	Cd(1)–Cl(1)	2.438(2)
Pt(1)–Se(1)	2.4595(7)	Cd(1)–Cl(1C)	2.438(2)
Pt(1)–Se(1A)	2.4916(7)	Cd(1)–Se(1)	2.6852(10)
Pt(1)–Cd(1)	3.3235(8)	Cd(1)–Se(1A)	2.6852(10)
Pt(1A)–Cd(1)	3.3235(8)		
Pt(1)–Se(1)–Pt(1A)	86.97(2)	P(2)–Pt(1)–Se(1A)	86.69(5)
Se(1)–Pt(1)–Se(1A)	83.08(3)	Cl(1)–Cd(1)–Cl(1C)	113.20(14)
Pt(1)–Se(1)–Cd(1)	80.35(2)	Cl(1)–Cd(1)–Se(1A)	114.16(7)
Pt(1A)–Se(1)–Cd(1)	79.78(2)	Cl(1C)–Cd(1)–Se(1A)	117.51(7)
P(1)–Pt(1)–P(2)	99.13(6)	Cl(1)–Cd(1)–Se(1)	117.51(7)
P(1)–Pt(1)–Se(1)	91.13(5)	Cl(1C)–Cd(1)–Se(1)	114.16(7)
P(2)–Pt(1)–Se(1)	169.60(5)	Se(1)–Cd(1)–Se(1A)	75.38(4)
P(1)–Pt(1)–Se(1A)	174.08(5)		

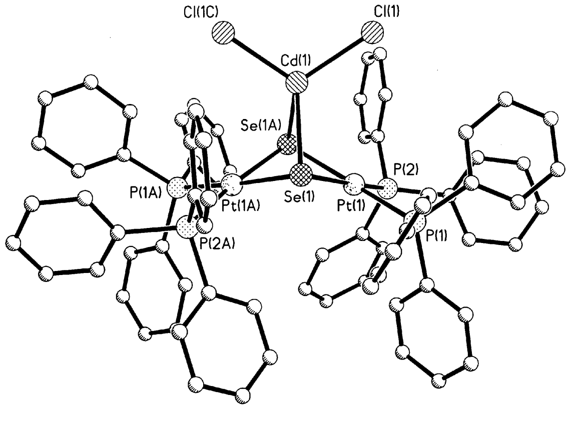

Fig. 3 Molecular structure of the neutral complex [$Pt_2(\mu_3\text{-}Se)_2(PPh_3)_4(CdCl_2)$] **11e**. The dichloromethane, water of solvation and hydrogen atoms on the phenyl rings are omitted for clarity.

behave identically under ESMS conditions. We are currently investigating the development of compound **11e** as a building block for multi-metallic materials, taking advantage of its spontaneous dissociation of chloride which provides an active site for coordination.

(c) Reactions between 1 and Group 13 (gallium, indium, thallium), Group 14 (germanium, lead) and Group 15 (antimony, bismuth) substrates. ESMS data for displacement reactions with Group 13, 14 and 15 complexes are reported in Tables 4, 5 and 6 respectively. All reactions shown in the tables were repeated on a preparative scale and the respective isolated products reported in the Experimental section.

Detection of [$Pt_2(\mu_3\text{-}Se)_2(PPh_3)_4(Pb)$]$^{2+}$ and {$Pt_2(\mu_3\text{-}Se)_2(PPh_3)_4[Pb(NO_3)]$}$^+$ (*m*/*z* 902 and 1866 respectively) in the reaction between **1** and $Pb(NO_3)_2$ illustrated the lability of the nitrate ligands. The re-run of this reaction after standing in solution over time showed a decrease in the intensity of the peak at *m*/*z* 1866 with a corresponding increase in that at *m*/*z* 902 that further suggested the ease of nitrate ligand dissociation. However, {[$Pt_2(\mu_3\text{-}Se)_2(PPh_3)_4]_2(Pb)$}$^{2+}$ was absent even when excess **1** was added. We have managed to isolate and fully characterize the product as {$Pt_2(\mu_3\text{-}Se)_2(PPh_3)_4[Pb(NO_3)]$}{$NO_3$} **13b** from the reaction performed on a preparative scale, and its structure is shown in Fig. 4. Compound **13b** consists of a {$Pb(NO_3)$} moiety resting on top of the metalloligand [$Pt_2(\mu\text{-}Se)_2(PPh_3)_4$] and the NO_3^- ligand is terminally bonded to the Pb atom. The second NO_3^- ligand is only weakly bonded. The bonding modes of the two NO_3^- ligands are further supported by IR data presented in the Experimental section. Among the four Pb–O bond lengths, only one [Pb(1)–O(1) 2.559 Å] suggests a strong Pb–O interaction. This NO_3^- ligand is best described as terminal and the coordination sphere of Pb(II) is [3 + 3]. The other three Pb–O bonds (aver. 2.817 Å), though not as strong as Pb(1)–O(1), are still within bonding

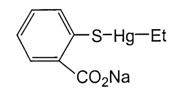

Sodium ethylmercurithiosalicylate
(thiomersal) **IV**

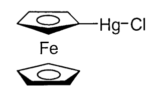

Ferrocenyl mercury chloride[26]
(HgFcCl) **V**

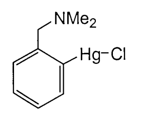

2-N,N-Dimethylaminomethylphenyl mercury chloride[29] [$HgCl(BzNMe_2)$] **VI**

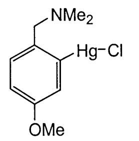

2-N,N-Dimethylaminomethyl(5-methoxy)phenyl mercury chloride[29] [$HgCl(p\text{-}OMe\text{-}BzNMe_2)$] **VII**

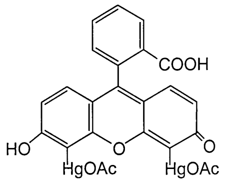

Fluorescein mercury acetate
(Fluores HgOAc) **VIII**

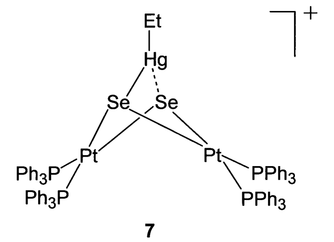

7

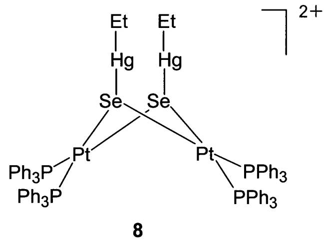

8

Table 4 ESMS data for reactions between $[Pt_2(\mu\text{-}Se)_2(PPh_3)_4]$ **1** and Group 13 substrates

Combinations	Cone voltage/V	Major ions (*m*/*z*, %)
$\mathbf{1} + Ga(NO_3)_3$	20	$\{\mathbf{1}[Ga(NO_3)]\}^{2+}$ (864, 100), $\{\mathbf{1}[Ga(NO_3)_2]\}^+$ (1790, 20)
	40	$\{\mathbf{1}[Ga(NO_3)]\}^{2+}$ (864, 80), $\{\mathbf{1}[Ga(NO_3)_2]\}^+$ (1790, 100)
	60	$\{\mathbf{1}[Ga(NO_3)]\}^{2+}$ (864, 36) $\{(\mathbf{1} - PPh_3)[Ga(NO_3)_2]\}^+$ (1794, 20), $\{\mathbf{1}[Ga(NO_3)_2]\}^+$ (1790, 100)
	80	$\{\mathbf{1}[Ga(NO_3)]\}^{2+}$ (864, 6) $\{(\mathbf{1} - PPh_3)[Ga(NO_3)_2]\}^+$ (1794, 80), $\{\mathbf{1}[Ga(NO_3)_2]\}^+$ (1790, 100)
$\mathbf{1} + InBr_3$	20	$[\mathbf{1}(InBr)]^2$ (896, 100), $[\mathbf{1}(InBr_2)]^+$ (1872, 30)
	40	$[\mathbf{1}(InBr)]^{2+}$ (896, 100), $[\mathbf{1}(InBr_2)]^+$ (1872, 80)
	60	$[\mathbf{1}(InBr)]^{2+}$ (896, 45), $[(\mathbf{1} - PPh_3)(InBr_2)]^+$ (1610, 15), $[\mathbf{1}(InBr_2)]^+$ (1872, 100)
	80	$[(\mathbf{1} - PPh_3)(InBr_2)]^+$ (1610, 85), $[\mathbf{1}(InBr_2)]^+$ (1782, 100)
$\mathbf{1} + Tl(NO_3)$	20–60	$[\mathbf{1}(Tl)]^+$ (1802, 100)

Table 5 ESMS data for reactions between $[Pt_2(\mu\text{-}Se)_2(PPh_3)_4]$ **1** and Group 14 substrates

Combinations	Cone voltage/V	Major ions (*m*/*z*, %)
$\mathbf{1} + GeI_4$	20	$[\mathbf{1}(GeI_2)]^{2+}$ (962, 80), $[\mathbf{1}(GeI_3)]^+$ (2051, 100)
	40	$[\mathbf{1}(GeI_2)]^{2+}$ (962, 26), $[(\mathbf{1} - PPh_3)(GeI_3)]^+$ (1789, 35), $[\mathbf{1}(GeI_3)]^+$ (2051, 100)
	80	$[(\mathbf{1} - 2PPh_3)(GeI_3)]^+$ (1527, 8), $[(\mathbf{1} - PPh_3)(GeI_3)]^+$ (1789, 100), $[\mathbf{1}(GeI_3)]^+$ (2051, 85)
$\mathbf{1} + Pb(NO_3)_2$	20	$[\mathbf{1}(Pb)]^{2+}$ (902, 100), $\{\mathbf{1}[Pb(NO_3)]\}^+$ (1866, 38)
	40	$[\mathbf{1}(Pb)]^{2+}$ (902, 100), $\{\mathbf{1}[Pb(NO_3)]\}^+$ (1866, 72)
	80	$[\mathbf{1}(Pb)]^{2+}$ (902, 10), $\{(\mathbf{1} - PPh_3)[Pb(NO_3)]\}^+$ (1604, 10), $\{\mathbf{1}[Pb(NO_3)]\}^+$ (1866, 100)

Table 6 ESMS data for reactions between $[Pt_2(\mu\text{-}Se)_2(PPh_3)_4]$ **1** and Group 15 substrates

Combinations	Cone voltage/V	Major ions (*m*/*z*, %)
$\mathbf{1} + SbCl_3$	20	$[\mathbf{1}(SbCl)]^{2+}$ (877, 100), $[\mathbf{1}(SbCl_2)]^+$ (1790, 15)
	40	$[\mathbf{1}(SbCl)]^{2+}$ (877, 100), $[\mathbf{1}(SbCl_2)]^+$ (1790, 67)
	60	$[\mathbf{1}(SbCl)]^{2+}$ (877, 56), $[(\mathbf{1} - PPh_3)(SbCl_2)]^+$ (1528, 5), $[\mathbf{1}(SbCl_2)]^+$ (1790, 100)
	80	$[\mathbf{1}(SbCl)]^{2+}$ (877, 16), $[(\mathbf{1} - PPh_3)(SbCl_2)]^+$ (1528, 45), $[\mathbf{1}(SbCl_2)]^+$ (1790, 100)
$\mathbf{1} + BiCl_3$	20	$[\mathbf{1}(BiCl)]^{2+}$ (921, 100), $[\mathbf{1}(BiCl_2)]^+$ (1877, 13)
	40	$[\mathbf{1}(BiCl)]^{2+}$ (921, 100), $[\mathbf{1}(BiCl_2)]^+$ (1877, 47)
	60	$[\mathbf{1}(BiCl)]^{2+}$ (921, 72), $[\mathbf{1}(BiCl_2)]^+$ (1877, 100)
	80	$[\mathbf{1}(BiCl)]^{2+}$ (921, 22), $[(\mathbf{1} - PPh_3)(BiCl_2)]^+$ (1615, 51), $[\mathbf{1}(BiCl_2)]^+$ (1877, 100)

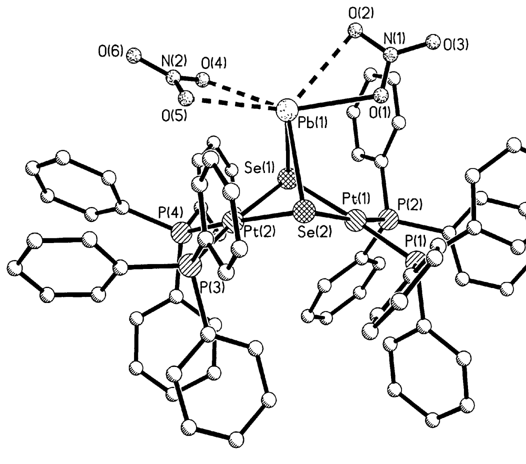

Fig. 4 Molecular structure of the cationic complex $\{Pt_2(\mu_3\text{-}Se)_2(PPh_3)_4[Pb(NO_3)]\}\{NO_3\}$ **13b**. The dichloromethane of solvation and hydrogen atoms on the phenyl rings are omitted for clarity.

distance when compared to a selection of $Pb–NO_3$ structures (<3 Å) obtained from the CCDC.[21] Upon coordination to the $\{Pb(NO_3)\}$ moiety, the $\{Pt_2Se_2\}$ core bends from planarity, giving a dihedral angle of 132.5°. Similar observations are found in the sulfur analogue, *viz.* $\{Pt_2(\mu_3\text{-}S)_2(PPh_3)_4[Pb(NO_3)]\}\{NO_3\}$,[22] and the structural parameters of these two structures are compared in Table 7. From the bond parameters, it can be observed that the coordinating nitrate ligand in **13b** adopts the terminal mode whereas that in the sulfur analogue prefers the chelating mode. This can be rationalized through the Lewis basicity of the selenium atoms in **13b** (over the sulfur atoms), thus causing the central lead atom to be more electron rich and less willing to accept additional donation from the nitrate ligand.

Conclusions

The ability of ESMS and its simplicity to monitor solution chemistry has been emphasized through successful displacement experiments demonstrated by $Pt_2(\mu\text{-}Se)_2(PPh_3)_4$ on a wide range of metal substrates. The resulting intermetallic aggregates are identified and subsequently confirmed by synthetic studies and single-crystal X-ray diffraction analyses. Full characterization of the products isolated from preparative scale syntheses corresponded to the respective species deduced from the ESMS data. These results suggest that there is a clear link between species observed by ESMS and isolable products. This emphasizes our belief that more synthetic chemists should take advantage of this ESMS-directed synthetic methodology for their materials. Our next target is to study the material properties of these intermetallic selenides, especially as precursors to opto-electronically active materials.

Experimental

Mass spectrometry

Samples for ESMS analysis were prepared by dissolving **1** and substrate (both 10–100 µg) in 1 mL MeOH. Electrospray mass spectra were obtained with a VG Platform II mass spectrometer with the methanol mobile phase driven at 0.02 mL min^{-1} using

Table 7 Comparison of selected bond lengths (Å) and angles (°) between compound **13b**·CH_2Cl_2 and its sulfur analogue[17]

$\{Pt_2(\mu_3\text{-}S)_2(PPh_3)_4[Pb(NO_3)]\}\{NO_3\}$		$\{Pt_2(\mu_3\text{-}Se)_2(PPh_3)_4[Pb(NO_3)]\}\{NO_3\}\cdot CH_2Cl_2$	
Pb(1)–S(1)	2.744(4)	Pb(1)–Se(1)	2.8567(12)
Pb(1)–S(2)	2.692(4)	Pb(1)–Se(2)	2.7825(12)
Pb(1)–O(1)	2.574(14)	Pb(1)–O(1)	2.559(9)
Pb(1)–O(2)	2.709(16)	Pb(1)–O(2)	2.883(12)
Pb(1)–O(4)	2.951(15)	Pb(1)–O(4)	2.860(8)
Pb(1)–O(5)	2.790(15)	Pb(1)–O(5)	2.790(7)
Pt(1)–S(1)	2.352(4)	Pt(1)–Se(1)	2.4535(10)
Pt(1)–S(2)	2.362(3)	Pt(1)–Se(2)	2.4710(10)
Pt(2)–S(1)	2.357(3)	Pt(2)–Se(1)	2.4864(11)
Pt(2)–S(2)	2.334(3)	Pt(2)–Se(2)	2.4685(11)
Mean Pt–P	2.296(6)	Mean Pt–P	2.292(3)
N(1)–O(1)	1.117(32)	N(1)–O(1)	1.221(14)
N(1)–O(2)	1.289(30)	N(1)–O(2)	1.254(16)
N(1)–O(3)	1.149(34)	N(1)–O(3)	1.237(14)
N(2)–O(4)	1.339(53)	N(2)–O(4)	1.262(11)
N(2)–O(5)	0.955(55)	N(2)–O(5)	1.248(10)
N(2)–O(6)	1.228(43)	N(2)–O(6)	1.222(10)
S(1)–Pb(1)–S(2)	68.5(1)	Se(1)–Pb(1)–Se(2)	69.99(3)
O(1)–Pb(1)–O(2)	46.5(6)	O(1)–Pb(1)–O(2)	45.3(3)
O(4)–Pb(1)–O(5)	35.2(30)	O(4)–Pb(1)–O(5)	44.7(2)
S(1)–Pb(1)–O(1)	104.7(4)	Se(1)–Pb(1)–O(1)	101.2(2)
S(1)–Pb(1)–O(2)	146.0(4)	Se(1)–Pb(1)–O(2)	130.5(3)
S(2)–Pb(1)–O(1)	89.4(5)	Se(2)–Pb(1)–O(1)	85.4(3)
S(2)–Pb(1)–O(2)	90.5(6)	Se(2)–Pb(1)–O(2)	108.7(3)
S(1)–Pt(1)–S(2)	80.9(1)	Se(1)–Pt(1)–Se(2)	82.12(3)
S(1)–Pt(2)–S(2)	81.4(1)	Se(1)–Pt(2)–Se(2)	81.51(4)
S(1)–Pt(1)–P(1)	91.7(1)	Se(1)–Pt(1)–P(1)	92.66(7)
S(2)–Pt(1)–P(2)	87.4(1)	Se(2)–Pt(1)–P(2)	86.66(7)
S(1)–Pt(2)–P(3)	86.2(1)	Se(1)–Pt(2)–P(3)	87.09(7)
S(2)–Pt(2)–P(4)	91.1(1)	Se(2)–Pt(2)–P(4)	90.84(7)
P(1)–Pt(1)–P(2)	100.0(1)	P(1)–Pt(1)–P(2)	98.58(9)
P(3)–Pt(2)–P(4)	101.4(1)	P(3)–Pt(2)–P(4)	100.39(9)
O(1)–N(1)–O(2)	120.2(21)	O(1)–N(1)–O(2)	117.6(13)
O(1)–N(1)–O(3)	124.7(6)	O(1)–N(1)–O(3)	122.2(15)
O(2)–N(1)–O(3)	114.2(25)	O(2)–N(1)–O(3)	119.3(16)
O(4)–N(2)–O(5)	101.1(44)	O(4)–N(2)–O(5)	117.8(9)
O(4)–N(2)–O(6)	100.8(33)	O(4)–N(2)–O(6)	120.2(10)
O(5)–N(2)–O(6)	147.4(52)	O(5)–N(2)–O(6)	122.0(10)
Dihedral angle Pt(1)–S(1)–S(2)–Pt(2)	132.2	Dihedral angle Pt(1)–Se(1)–Se(2)–Pt(2)	132.5

a Thermo Separation products SpectraSystem P1000 LC pump. Samples were injected *via* a Rheodyne valve fitted with a 10 μL sample loop. The source temperature was 60 °C. The capillary potential tip was 3500 V, with nitrogen used both as a drying and a nebulizing gas. The skimmer cone voltage was usually 5 V when clean parent ions were required, and was varied up to 80 V to investigate fragmentation processes. Peaks were assigned from the *m*/*z* values and from the isotope distribution patterns that were simulated using the ISOTOPE program.[23] The *m*/*z* values given are for the most intense peak in the envelope in each case.

Materials

The substrates used were $AuCl(PPh_3)$,[24] $Au(anpy)Cl_2$ (anpy = cyclometallated 2-anilinopyridyl),[25] $Au(tolpy)Cl_2$ (tolpy = cyclometallated *p*-tolylpyridyl),[26] $Au(tolpyH)Cl_3$ (tolpyH = *p*-tolylpyridine),[26] HgFcCl,[27] $HgCl_2(PPh_3)_2$,[28] $HgBr_2(dppe)$,[29] $HgCl(BzNMe_2)$,[30] HgCl(*p*-$OMeBzNMe_2$),[30] $[NMe_4][AuCl_4]$ is commercially available from Strem; HgPhCl from Fluka; $EtHgSC_6H_4CO_2Na$ (thiomersal) and $SbCl_3$ from BDH; $Ga(ClO_4)_3$, $Hg(ClO_4)_2$, fluorescein$[Hg(OAc)]_2$ and $InBr_3$ from Aldrich; $Ga(NO_3)_3$ and GeI_4 from Johnson Matthey; $TlNO_3$ and $Pb(NO_3)_2$ from Merck; and $BiCl_3$ from TCI. **CAUTION**: perchlorate salts combined with organic ligands are potentially explosive and should be handled in small quantity and with the necessary precautions,[31] Hg(II) compounds are highly toxic and any skin contact must be avoided. A modified preparation of $Pt_2(\mu\text{-}Se)_2(PPh_3)_4$ **1** was adapted from our recent report.[6] All reactions were performed under a positive pressure of purified argon unless otherwise stated, and solvents were distilled and degassed before use. ^1H NMR spectra were recorded at 300 MHz at 25 °C on a Bruker ACF 300 spectrometer. The ^{31}P NMR spectra were recorded at 121.39 MHz with 85% H_3PO_4 as external reference, PF_6^- resonances at around −144 ppm [heptet, ^1J(P–F) = 713 Hz] are omitted from ^{31}P NMR reports for clarity. Infrared spectra were recorded in the range 4000–400 cm^{-1}, on a Perkin-Elmer FTIR spectrometer. Elemental analyses were performed by the microanalytical laboratory of the Department of Chemistry at the National University of Singapore.

Synthesis of di-protonated $[Pt_2(\mu\text{-}Se)_2(PPh_3)_4]$

$[Pt_2(\mu\text{-}SeH)_2(PPh_3)_4][ClO_4]_2$ (3). An aqueous solution of $Ga(ClO_4)_3$ (14.5 mg, 2.20 μL, 0.0395 mmol) was added to a brown suspension of **1** (57.8 mg, 0.0362 mmol) in MeOH (20 mL). The resulting orange suspension was stirred for 24 h and filtered. The solid was washed successively with 100 mL portions of deionized water and Et_2O, and dried under vacuum yielding an orange powder of **3** (0.0514 g, 79%). Found: C, 47.7; H, 3.4; P, 6.1. Calc. for $C_{72}H_{62}Cl_2O_8Se_2P_4Pt_2$: C, 48.1; H, 3.5; P, 6.9%. ^{31}P-{^1H} NMR ($CDCl_3$): δ_p 5.4 [t, ^1J(P–Pt) = 3910 Hz]. ^1H NMR ($CDCl_3$): δ_H 1.25 (s, 2 H, 2 SeH), 7.10–7.80 (m, 60 H, 12 C_6H_5).

$[Pt_2(\mu\text{-}SeH)_2(PPh_3)_4][PF_6]_2$ (3a). HPF_6 (9.2 mg, 1.52 μL, 0.0631 mmol) was added to a brown suspension of **1** (43.2 mg, 0.0270 mmol) in MeOH (20 mL). The resulting orange–brown suspension was stirred for 1 h and filtered. The solid was washed successively with 100 mL of Et_2O, and dried under vacuum yielding an orange powder of **3a** (0.0460 g, 90%). Found: C, 45.4; H, 3.2; P, 9.1. Calc. for $C_{72}H_{62}F_{12}Se_2P_6Pt_2$: C, 45.8; H, 3.3; P, 9.8%. ^{31}P-{^1H} NMR ($CDCl_3$): δ_P 5.4 [t, ^1J(P–Pt) = 3910 Hz]. ^1H NMR ($CDCl_3$): δ_H 1.25 (s, 2 H, 2 SeH), 7.10–7.80 (m, 60 H, 12 C_6H_5). Alternatively, **3a** can be prepared by the addition of HCl to a MeOH suspension of **1** and subsequent metathesis with NH_4PF_6 (48% yield).

Synthesis of heterometallic aggregates

{$Pt_2(\mu_3\text{-}Se)_2(PPh_3)_4[Au(PPh_3)]$}{$PF_6$} (10a). AuCl($PPh_3$) (15.8 mg, 0.0319 mmol) was added to a brown suspension of **1** (50.4 mg, 0.0316 mmol) in MeOH (20 mL). The resulting orange solution was stirred for 3 h, after which excess NH_4PF_6 (10.0 mg, 0.0614 mol) was introduced to give an orange–brown suspension. After stirring for 1 h, deionized water (50 mL) was added to induce precipitation. The suspension was filtered, the solid washed successively with 100 mL portions of deionized water and Et_2O, and dried under vacuum yielding an orange–brown powder of **10a** (0.0358 g, 52%). Found: C, 49.0; H, 3.3; P, 8.1. Calc. for $C_{90}H_{75}F_6Se_2P_6AuPt_2$: C, 49.1; H, 3.4; P, 8.4%. ^{31}P-{^1H} NMR ($CDCl_3$): δ_P 19.0 [t, ^1J(P–Pt) = 3117 Hz], 33.6 [s, 1 P (PPh_3 on Au)].

{$Pt_2(\mu_3\text{-}Se)_2(PPh_3)_4[Au(anpy)]$}{$PF_6$}$_2$ (10b). Following a similar procedure as described for **10a**, Au(anpy)Cl_2 **I** (12.6 mg, 0.0288 mmol) and **1** (45.8 mg, 0.0287 mmol) gave an orange powder of **10b** (0.0313 g, 48%). Found: C, 45.0; H, 3.1; P, 8.4. Calc. for $C_{84}H_{70}F_{12}Se_2NP_6AuPt_2$: C, 44.8; H, 3.1; P, 8.2%. ^{31}P-{^1H} NMR ($CDCl_3$): δ_P 13.5 [t, ^1J(P–Pt) = 3273 Hz].

[$Pt_2(\mu_3\text{-}Se)_2(PPh_3)_4(HgPh)$][$PF_6$] (11a). Following a similar procedure as described for **10a**, HgPhCl (9.4 mg, 0.0300 mmol) and **1** (47.8 mg, 0.0299 mmol) gave an orange–brown powder of **11a** (0.0388 g, 64%). Found: C, 46.3; H, 3.2; P, 7.5. Calc. for $C_{78}H_{65}F_6Se_2P_5HgPt_2$: C, 46.4; H, 3.2; P, 7.7%. ^{31}P-{^1H} NMR ($CDCl_3$): δ_P 19.6 [t, ^1J(P–Pt) = 3120 Hz].

[$Pt_2(\mu_3\text{-}Se)_2(PPh_3)_4HgEt$][$PF_6$] (11b). Following a similar procedure as described for **10a**, $EtHgSC_6H_4CO_2Na$ **IV** (12.2 mg, 0.0301 mmol) and **1** (47.4 mg, 0.0297 mmol) gave a yellow powder of **11b** (0.0178 g, 30%). Found: C, 44.9; H, 3.2; P, 7.8. Calc. for $C_{74}H_{65}F_6Se_2P_5HgPt_2$: C, 45.1; H, 3.3; P, 7.9%. ^{31}P-{^1H} NMR ($CDCl_3$): δ_P 20.1 [t, ^1J(P–Pt) = 3136 Hz].

[$Pt_2(\mu_3\text{-}Se)_2(PPh_3)_4HgFc$][$PF_6$] (11c). Following a similar procedure as described for **10a**, HgFcCl **V** (13.4 mg, 0.0318 mmol) and **1** (50.0 mg, 0.0313 mmol) gave an orange–brown powder of **11c** (0.0423 g, 64%). Found: C, 46.0; H, 3.2; P, 7.0. Calc. for $C_{82}H_{69}F_6Se_2P_5FeHgPt_2$: C, 46.3; H, 3.3; P, 7.3%. ^{31}P-{^1H} NMR ($CDCl_3$): δ_P 19.3 [t, ^1J(P–Pt) = 3117 Hz].

{[$Pt_2(\mu_3\text{-}Se)_2(PPh_3)_4]_2Hg$}{$ClO_4$}$_2$ (11d). Following a similar procedure as described for **10a** (with the exclusion of metathesis by NH_4PF_6), $Hg(ClO_4)_2\cdot H_2O$ (5.8 mg, 0.0145 mmol) and **1** (46.6 mg, 0.0292 mmol) gave an orange–brown powder of **11d** (0.0382 g, 36%). Found: C, 48.0; H, 3.4; P, 6.6. Calc. for $C_{144}H_{120}Cl_2O_8Se_4P_8HgPt_2$: C, 48.1; H, 3.4; P, 6.9%. ^{31}P-{^1H} NMR ($CDCl_3$): δ_P 18.5 [t, ^1J(P–Pt) = 3113 Hz].

[$Pt_2(\mu_3\text{-}Se)_2(PPh_3)_4(CdCl_2)$] (11e). $CdCl_2$ (21.0 mg, 0.1145 mmol) was added to a brown suspension of **1** (182.0 mg, 0.1140 mmol) in MeOH (30 mL). An immediate bright yellow suspension resulted and it was stirred for 2 h. The suspension was filtered, the solid washed successively with 30 mL of MeOH and 100 mL of Et_2O, and dried under vacuum yielding a bright yellow powder of **11e** (0.1356 g, 67%). Found: C, 48.5; H, 3.3; P, 6.7. Calc. for $C_{72}H_{60}Cl_2Se_2P_4CdPt_2$: C, 48.6; H, 3.4; P, 7.0%. ^{31}P-{^1H} NMR ($CDCl_3$): δ_P 21.1 [t, ^1J(P–Pt) = 3047 Hz].

{$Pt_2(\mu_3\text{-}Se)_2(PPh_3)_4[Ga(NO_3)_2]$}{$PF_6$} (12a). Following a similar procedure as described for **10a**, $Ga(NO_3)_3$ (8.2 mg, 0.0321 mmol) and **1** (50.0 mg, 0.0313 mmol) gave a brown powder of **12a** (0.0263 g, 43%). Found: C, 44.5; H, 3.0; N, 1.2; P, 7.7. Calc. for $C_{72}H_{60}F_6O_6Se_2N_2P_5GaPt_2$: C, 44.7; H, 3.1; N, 1.4; P, 8.0%. ^{31}P-{^1H} NMR ($CDCl_3$): δ_P 18.7 [t, ^1J(P–Pt) = 3216 Hz].

[$Pt_2(\mu_3\text{-}Se)_2(PPh_3)_4InBr_2$][$PF_6$] (12b). Following a similar procedure as described for **10a**, $InBr_3$ (11.2 mg, 0.0316 mmol) and **1** (50.0 mg, 0.0313 mmol) gave a brown powder of **12b** (0.0242 g, 38%). Found: C, 42.9; H, 3.0; P, 7.6. Calc. for $C_{72}H_{60}Br_2F_6Se_2P_5InPt_2$: C, 42.9; H, 3.0; P, 7.7%. ^{31}P-{^1H} NMR ($CDCl_3$): δ_P 17.7 [t, ^1J(P–Pt) = 3201 Hz].

[$Pt_2(\mu_3\text{-}Se)_2(PPh_3)_4Tl$][$NO_3$] (12c). Following a similar procedure as described for **10a** (with the exclusion of metathesis by NH_4PF_6), $TlNO_3$ (8.4 mg, 0.0315 mmol) and **1** (50.0 mg, 0.0313 mmol) gave a brown powder of **12c** (0.0242 g, 41%). Found: C, 46.3; H, 3.2; P, 6.3. Calc. for $C_{72}H_{60}O_3Se_2NP_4Pt_2Tl$: C, 46.4; H, 3.2; P, 6.6%. ^{31}P-{^1H} NMR ($CDCl_3$): δ_P 20.1 [t, ^1J(P–Pt) = 3017 Hz].

[$Pt_2(\mu_3\text{-}Se)_2(PPh_3)_4GeI_3$][$PF_6$] (13a). Following a similar procedure as described for **10a**, GeI_4 (19.0 mg, 0.0327 mmol) and **1** (50.0 mg, 0.0313 mmol) gave an orange powder of **13a** (0.0188 g, 27%). Found: C, 39.3; H, 2.8; P, 7.0. Calc. for $C_{72}H_{60}F_6I_3Se_2P_5GePt_2$: C, 39.4; H, 2.8; P, 7.1%. ^{31}P-{^1H} NMR ($CDCl_3$): δ_P 19.6 [t, ^1J(P–Pt) = 3043 Hz].

{$Pt_2(\mu_3\text{-}Se)_2(PPh_3)_4[Pb(NO_3)]$}{$NO_3$} (13b). Following a similar procedure as described for **10a** (with the exclusion of metathesis by NH_4PF_6), $Pb(NO_3)_2$ (10.5 mg, 0.0317 mmol) and **1** (50.0 mg, 0.0313 mmol) gave a brown powder of **13b** (0.0208 g, 34%). Found: C, 44.6; H, 3.1; N, 1.4; P, 6.1. Calc. for $C_{72}H_{60}O_6Se_2N_2P_4PbPt_2$: C, 44.8; H, 3.1; N, 1.5; P, 6.4%. ^{31}P-{^1H} NMR ($CDCl_3$): δ_P 15.9 [t, ^1J(P–Pt) = 3143 Hz]. $\nu(NO_3^-)$ in CH_2Cl_2: 1381 (uncoordinated NO_3^-), 1272 (coordinated NO_3^-) cm^{-1}.

[$Pt_2(\mu_3\text{-}Se)_2(PPh_3)_4SbCl_2$][$PF_6$] (14a). Following a similar procedure as described for **10a**, $SbCl_3$ (7.3 mg, 0.0320 mmol) and **1** (50.0 mg, 0.0313 mmol) gave an orange–brown powder of **14a** (0.0400 g, 66%). Found: C, 44.7; H, 3.1; P, 8.1. Calc. for $C_{72}H_{60}Cl_2F_6Se_2P_5Pt_2Sb$: C, 44.7; H, 3.1; P, 8.0%. ^{31}P-{^1H} NMR ($CDCl_3$): δ_P 16.8 [t, ^1J(P–Pt) = 3239 Hz].

[$Pt_2(\mu_3\text{-}Se)_2(PPh_3)_4BiCl_2$][$PF_6$] (14b). Following a similar procedure as described for **10a**, $BiCl_3$ (10.0 mg, 0.0317 mmol) and **1** (50.0 mg, 0.0313 mmol) gave an orange–brown powder of **14b** (0.0315 g, 50%). Found: C, 42.7; H, 2.9; P, 7.4. Calc. for $C_{72}H_{60}Cl_2F_6Se_2P_5BiPt_2$: C, 42.8; H, 3.0; P, 7.7%. ^{31}P-{^1H} NMR ($CDCl_3$): δ_P 11.8 [t, ^1J(P–Pt) = 3235 Hz].

Crystal structure determination and refinement

Suitable single crystals of [$Pt_2(\mu\text{-}SeH)_2(PPh_3)_4$][$PF_6$]$_2$ **3**, [$Pt_2(\mu_3\text{-}Se)_2(PPh_3)_4(CdCl_2)$] **11e** and {$Pt_2(\mu_3\text{-}Se)_2(PPh_3)_4[Pb(NO_3)]$}{$NO_3$} **13b** for structure determination were obtained by layering a CH_2Cl_2 solution of each compound with hexane. The data collections were performed on a Bruker AXS SMART diffractometer, equipped with a CCD area-detector using Mo-Kα radiation (λ = 0.71073 Å). The software SMART[32] was used for collecting frames of data, indexing reflections, and the determination of lattice parameters, SAINT[32] for integration of intensity of reflections and scaling, SADABS[33] for empirical absorption correction, and SHELXTL[34] for space group and structure determination, refinements, graphics, and structure reporting. The structures were refined by full-matrix least squares on F^2 with anisotropic thermal parameters for non-

Table 8 Crystallographic data for complexes **3**, **11e** and **13b**

	3	**11e**·CH_2Cl_2·$2H_2O$	**13b**·CH_2Cl_2
Formula	$C_{72}H_{62}Cl_2O_8Se_2P_4Pt_2$	$C_{73}H_{66}Cl_4O_2Se_2P_4CdPt_2$	$C_{73}H_{62}Cl_2O_6Se_2N_2P_4PbPt_2$
Formula weight	1798.10	1901.44	2013.32
Crystal system	Triclinic	Monoclinic	Triclinic
Space group	*P*-1	*P*2/*n*	*P*-1
a/Å	12.8006(12)	17.2097(12)	12.1770(2)
b/Å	13.6942(12)	11.8079(9)	16.8986(3)
c/Å	24.217(2)	17.6063(12)	17.5281(3)
α/°	103.072(2)	90	75.202(1)
β/°	93.836(2)	105.918(2)	87.163(1)
γ/°	114.111(2)	90	89.219(1)
V/Å^3	3713.3(6)	3440.6(4)	3482.9(1)
Z	2	2	2
μ/mm^{-1}	4.952	5.714	7.685
T/K	223(2)	223(2)	223(2)
No. of total reflections	30240	19576	16730
No. of unique reflections [$I > 2\sigma(I)$] (R_{int})	13071 (0.0627)	6053 (0.0812)	11571 (0.0417)
R	0.0599	0.0409	0.0519
wR	0.1441	0.0798	0.0853

hydrogen atoms, unless otherwise indicated [$R_1 = \Sigma||F_o| - |F_c||/\Sigma|F_o|$, and $wR_2 = \{\Sigma[w(F_o^2 - F_c^2)^2]/\Sigma[w(F_o^2)^2]\}^{1/2}$ (where $w^{-1} = \sigma^2(F_o^2) + (aP)^2 + (bP)$]. A summary of parameters for the data collections and refinements is given in Table 8.

CCDC reference numbers 165971–165973.

See http://www.rsc.org/suppdata/dt/b1/b104996h/ for crystallographic data in CIF or other electronic format.

Acknowledgements

The authors acknowledge the National University of Singapore (NUS) for support (Grant RP 3992749) and J. S. L. Y. thanks NUS for a research scholarship and for attachment to the University of Waikato. W. H. thanks the University of Waikato and the New Zealand Lottery Grants Board for financial assistance, and Johnson Matthey plc for a generous loan of platinum. We thank G. K. Tan for her assistance with the X-ray analysis.

References

1 J. B. Fenn, M. Mann, C. K. Meng, S. F. Wong and C. M. Whitehouse, *Science*, 1989, **246**, 64; J. B. Fenn, M. Mann, C. K. Meng, S. F. Wong and C. M. Whitehouse, *Mass Spectrom. Rev.*, 1990, **9**, 37; R. B. Cole, *Electrospray Ionisation Mass Spectrometry; Fundamentals, Instrumentation and Applications*, Wiley-Interscience, New York, 1997; G. J. Langley and G. A. Mills, *Educ. Chem.*, 1997, 14; R. Bakhtiar, S. A. Hofstadler and R. D. Smith, *J. Chem. Educ.*, 1996, **73**, A118; M. Przybylski and M. O. Glocker, *Angew. Chem., Int. Ed. Engl.*, 1996, **35**, 807.

2 B. F. G. Johnson and J. S. McIndoe, *Coord. Chem. Rev.*, 2000, **200–202**, 901; I. I. Stewart, *Spectrochim. Acta B*, 1999, **54**, 1649; W. Henderson, B. K. Nicholson and L. J. McCaffrey, *Polyhedron*, 1998, **17**, 4291; C. E. C. A. Hop and R. Bakhtiar, *J. Chem. Educ.*, 1996, **73**, A165; R. Colton, A. D'Agostino and J. C. Traeger, *Mass Spectrom. Rev.*, 1995, **14**, 79.

3 L. J. McCaffrey, W. Henderson, B. K. Nicholson, J. E. Mackay and M. B. Dinger, *J. Chem. Soc., Dalton Trans.*, 1997, 2577.

4 S.-W. A. Fong, W. T. Yap, J. J. Vittal, A. G. Oliver, C. E. F. Rickard, W. Henderson and T. S. A. Hor, *J. Chem. Soc., Dalton Trans.*, 2001, 1986.

5 S.-W. A. Fong and T. S. A. Hor, *J. Chem. Soc., Dalton Trans.*, 1999, 639.

6 J. S. L. Yeo, J. J. Vittal, W. Henderson and T. S. A. Hor, *J. Chem. Soc., Dalton Trans.*, 2001, 315.

7 J. S. L. Yeo, J. J. Vittal, W. Henderson and T. S. A. Hor, unpublished work.

8 A. Bencini and S. Midollini, *Coord. Chem. Rev.*, 1992, **120**, 87; L. C. Roof and J. W. Kolis, *Chem. Rev.*, 1993, **93**, 1037.

9 R. R. Gukathasan, R. H. Morris and A. Walker, *Can. J. Chem.*, 1983, **61**, 2490; C. E. Briant, C. J. Gardner, T. S. A. Hor, N. D. Howells and D. M. P. Mingos, *J. Chem. Soc., Dalton Trans.*, 1984, 2645.

10 P. K. Khanna, C. P. Morley, M. B. Hursthouse, K. M. A. Malik and O. W. Howarth, *Heteroatom. Chem.*, 1995, **6**, 519.

11 S.-W. A. Fong, J. J. Vittal, W. Henderson, T. S. A. Hor, A. G. Oliver and C. E. F. Rickard, *Chem. Commun.*, 2001, 421.

12 M. Peruzzini, I. De Los Rios and A. Romerosa, *Prog. Inorg. Chem.*, 2001, **49**, 169.

13 A. Bencini, M. D. Vaira, R. Morassi and P. Stoppioni, *Polyhedron*, 1996, **15**, 2079.

14 U. Abram, K. Ortner, R. Gust and K. Sommer, *J. Chem. Soc., Dalton Trans.*, 2000, 735; K. Ortner and U. Abram, *Polyhedron*, 1999, **18**, 749; U. Abram, J. Mack, K. Ortner and M. Müller, *J. Chem. Soc., Dalton Trans.*, 1998, 1011.

15 E. S. Lang, M. Dahmer and U. Abram, *Acta Crystallogr., Sect. C*, 1999, **55**, 854; M. Takahashi, N. Robertson, R. J. H. Clark and A. E. Underhill, *Polyhedron*, 1999, **18**, 1545.

16 P. J. Craig, *Comprehensive Organometallic Chemistry*, ed. G. Wilkinson, Pergamon Press, Oxford, United Kingdom, 1982, vol. 2, ch. 18, p. 986.

17 L. J. McCaffrey, W. Henderson and B. K. Nicholson, *Polyhedron*, 1998, **17**, 221.

18 C. E. Briant, T. S. A. Hor, N. D. Howells and D. M. P. Mingos, *J. Chem. Soc., Chem. Commun.*, 1983, 1118.

19 Z. Li, Z.-H. Loh, S.-W. A. Fong, Y. K. Yan, W. Henderson, K. F. Mok and T. S. A. Hor, *J. Chem. Soc., Dalton Trans.*, 2000, 1027.

20 W. Henderson and C. Evans, *Inorg. Chim. Acta*, 1999, **294**, 183.

21 Structures from the Cambridge Crystallographic Data Centre (CCDC) with deposition codes MAKFAF, CUKZEN, DOBZIDIO, FICQOX, FILDIN, HAYSIJ, JUCCEP, KEJWVR, LIFZIJ and PIBLVH.

22 M. Zhou, Y. Xu, C.-F. Lam, L.-L. Koh, K. F. Mok, P.-H. Leung and T. S. A. Hor, *Inorg. Chem.*, 1993, **32**, 4660.

23 L. J. Arnold, *J. Chem. Educ.*, 1992, **69**, 811.

24 M. I. Bruce, B. K. Nicholson and O. B. Shawkataly, *Inorg. Synth.*, 1989, **26**, 325.

25 Y. Fuchita, H. Ieda, A. Kayama, J. Kinoshita-Nagaoka, H. Kawano, S. Kameda and M. Mikuriya, *J. Chem. Soc., Dalton Trans.*, 1998, 4095.

26 W. Henderson, B. K. Nicholson, S. J. Faville, D. Fan and J. D. Ranford, *J. Organomet. Chem.*, 2001, **631**, 41.

27 R. W. Fish and M. Rosenblum, *J. Org. Chem.*, 1965, **30**, 1253.

28 G. B. Deacon and B. O. West, *J. Inorg. Nucl. Chem.*, 1962, **24**, 169.

29 N. A. Bell and L. A. Nixon, *Thermochim. Acta*, 1973, **6**, 275.

30 V. Baliah and P. Subbarayan, *J. Indian Chem. Soc.*, 1963, **40**, 638.

31 W. C. Wolsey, *J. Chem. Educ.*, 1973, **50**, A335.

32 SMART & SAINT Software Reference Manuals, version 4.0, Siemens Energy & Automation, Inc., Analytical Instrumentation, Madison, WI, 1996.

33 G. M. Sheldrick, SADABS, software for empirical absorption correction, University of Göttingen, 1993.

34 G. M. Sheldrick, SHELXTL, version 5.03, Siemens Energy & Automation, Inc., Analytical Instrumentation, Madison, WI, 1996.